Int. J. Electrochem. Sci., 13 **(2018)** 7765 – 7777, doi: 10.20964/2018.08.56

International Journal of
ELECTROCHEMICAL
SCIENCE
www.electrochemsci.org

Surface Analysis and Electrochemical Corrosion Behavior of Anodic Oxide Films on Pure Titanium

Ruijia Diao, Ju Rong, Xiao Wang, Yuhan Yao, Zhaolin Zhan[*]*, Xiaohua Yu*[*]

Faculty of Materials Science and Engineering, Kunming University of Science and Technology, Kunming 650093, China.
[*]E-mail: zl_zhan@sohu.com, xiaohua_y@163.com

Received: 10 April 2018 / *Accepted:* 7 June 2018 / *Published:* 5 July 2018

Anodic oxide films were formed on commercially pure titanium by using a sulfuric acid anodizing process. The surface characteristics and corrosion behavior were evaluated via atomic force microscopy, X-ray photoelectron spectroscopy, polarization curves, electrochemical impedance spectroscopy, and scanning electron microscopy. The results revealed the hill-and-valley-like topography of, and nano-scale holes occurring in, the anodic oxide film. These holes increased in size and the oxidation degree of the film improved with increasing potential. Furthermore, the electrochemical test results revealed that the corrosion resistance of the film depends mainly on the dense inner oxide film. The oxide film obtained at high potential is less susceptible to corrosion compared with those formed at low potentials. The possible corrosion process of the oxide film is discussed. We believe that the corrosion of the film is closely correlated with the action of Cl^- ions. Defects on the film surface immersed in a NaCl solution will be damaged first, due to the invasion of Cl^-, leading to the formation of corrosion holes. Micro-cracks will form when adjacent holes become interconnected via corrosion.

Keywords: Anode oxidation; titanium oxide film; electrochemical characterization; corrosion resistance

1. INTRODUCTION

Anodic oxidation is a simple and low-temperature surface treatment commonly employed to thicken the oxide film on Titanium (Ti) and its alloys. This treatment improves the corrosion or wear resistance, external features, and the ability for adhesive bonding of the film [1–3]. Anodization of Ti and its alloys has been used in several fields, such as corrosion protection [4,5], solar energy conversion [6,7], batteries [8], photo-catalytic engineering [9], and biomedical engineering [10,11].

The suitability of anodized titanium for specific applications depends on the surface features, structure, and composition of the coating [12]. A study of the titanium oxide (TiOx) film surface, which provides insights into tailoring of the TiOx film for specific applications, is therefore essential.

The use of Ti and its alloys in various fields depends on the corrosion resistance of these materials. This resistance, in turn, depends on the thin, stable, inert, and self-adherent passive oxide film (formed on the surface), which inhibits corrosion in highly oxidizing environments [13]. The corrosion of Ti and its alloys has been extensively investigated. For example, Fadl-allah and Mohsen [1] investigated the corrosion behavior of commercially pure Ti in sulfuric and phosphoric acid solutions. Ningshen et al. [13] investigated the corrosion performance of Ti–Ni–Pd–Ru–Cr alloy in a NaCl solution, the corrosion behavior of this anodic film in the electrolyte. However, the governing corrosion mechanism of these materials has scarcely been investigated.

Therefore, in this work, an anodic oxide film was formed on the surface of pure Ti (TA2) by using a sulfuric acid anodizing process. The surface topography and chemical composition of the film were determined via atomic force microscopy and X-ray photoelectron spectroscopy (XPS), respectively. The prepared samples were then immersed in a Cl^-–containing solution, under an open circuit potential. Subsequently, the corrosion characteristics and properties of the TiOx films were evaluated via scanning electron microscopy (SEM), polarization curves, and electrochemical impedance spectroscopy (EIS). The oxide capacitance characterizing the relationship with the oxide thickness was calculated by the parallel plate capacitor model [12]. The present study focuses on the corrosion behavior of these films in an electrochemical etching solution. In addition, a possible corrosion mechanism is discussed.

2. EXPERIMENTAL

The chemical composition of the pure Ti used in this work is summarized in Table 1. The material was cut into 100 mm × 25 mm × 0.1 mm specimens, which were subsequently ground with 1000–2000 grit SiC paper, and ultrasonically cleaned with acetone and distilled water. These specimens were then electrochemically polished in a 0.5 M sulfuric acid solution at 25°C. The specimen and graphite sheet, designated as the cathode and anode, respectively, were subjected to a constant potential for 3 min, rinsed in distilled water, and dried in an oven.

Table 1. Chemical composition of TA2

Element	O	N	C	H	Fe	Si	Ti
Mass fraction (%)	0.15	0.05	0.05	<0.015	<0.30	<0.15	Balance

Using a regulated DC power supply, the polished specimens were anodized at room temperature in a 1.84 M sulfuric acid electrolyte solution containing methyl sulfonic acid. The passive films were formed after 1800 s at anodization potentials of 5 V, 25 V, and 50 V.

The three-dimensional surface profiles of the anodic oxide films were obtained by using an atomic force microscope (AFM, Nanoscope V, MultiMode®8, Bruker). In addition, the composition of each film was determined via X-ray photoelectron spectroscopy (XPS, ULVAC-Physical Electronics), using MgKα radiation. The corresponding peak-fitting procedure was performed using the ULVAC-PHI MultiPak 9.3 software, and the spectral positions were all corrected by normalizing the C1s spectrum at 284.6 eV.

The anodized specimens were immersed for 30 h in a 3.5 wt.% NaCl solution under an open circuit potential and potentiodynamic polarization curves were obtained during this immersion. Measurements were performed at a scanning rate of 1 mV/S. EIS was conducted at room temperature using a CHI760E electrochemical workstation in a three-electrode cell containing the NaCl solution. The specimen (surface area: 1 cm^2) was used as the working electrode; a saturated calomel reference electrode and a platinum counter electrode constituted the other electrodes in the cell. The EIS measurements were performed over a frequency range of 100 kHz–0.01 Hz, and at a perturbation amplitude of 5 mV. An initial delay of 300 s was used to obtain a stable testing system [14]. The corrosion morphologies of the specimens immersed for 30 h in a 3.5 w.t% NaCl solution were characterized using a Phillips XL30 scanning electron microscope.

3. RESULTS AND DISCUSSION

3.1. Surface characterization of the oxide film

The hill-and-valley-like topographies of the anodic oxide film formed in the H_2SO_4 solution are shown in the atomic force microscopy (AFM) images of Fig. 1. The film formed at an oxidation potential of 5 V exhibited uniform hill morphology (Fig. 1a), whereas a coarse and uneven hill-and-valley-like topography, with uniformly sized nano-scale holes in the center of the hills, was obtained at 25 V (Fig. 1b). When the potential was increased to 50 V (Fig. 1c), these holes transformed into concave holes on the valleys. This porous morphology has been attributed to the gas evolution [15,16] that accompanies hill formation. A compressive stress, generated by the swelling and extrusion of these hills, leads, in turn, to the formation of micro-cracks. These cracks will then be replaced by pores when the energy in the films increases with further increases in the voltage.

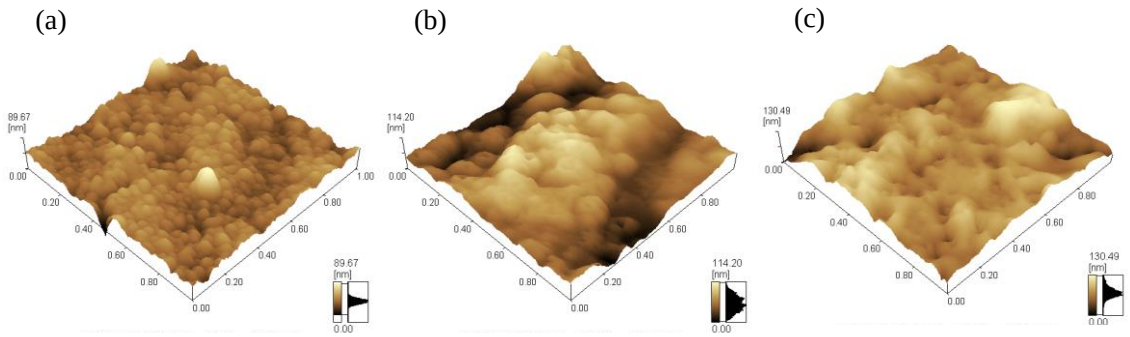

Figure 1. Atomic force microscope (AFM) images of the anodic oxide film formed at anodization potentials of (a) 5 V, (b) 25 V, and (c) 50 V

Figure 2 shows a full XPS spectrum of the anodic oxide film formed at each oxidation potential. As the figure shows, the elements Ti, O and C appear in the surface layer of each film. The C1s peaks result from contamination of the specimens.

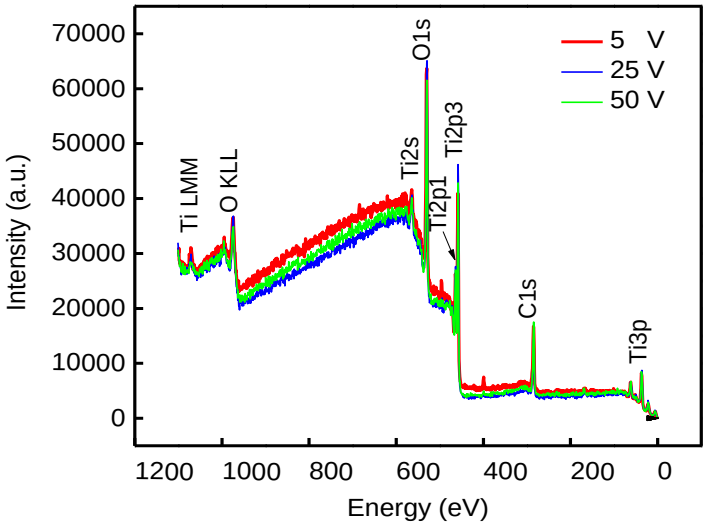

Figure 2. XPS survey spectrum of the anodic oxide film formed on Ti

The Ti2p peaks in the XPS spectra are decomposed into Ti2p3/2 and Ti2p1/2, depending on the electron spin-orbit coupling. Figure 3 shows the Ti2p survey spectrum of the film as a function of the potential applied to pure Ti. At an anodic oxidation potential of 5 V, the oxide film consists mainly of TiO_2, a small amount of Ti_2O_3, Ti metal, and titanium hydroxide (Fig. 3a). The presence of trace Ti metal indicates that the metal surface is only partially oxidized [17]. Figure 3b and c show the Ti2p peaks of the film formed at potentials of 25 and 50 V. Consistent with previous studies [4,18], doublet peaks occurred at binding energies of 458.2 and 463.9 eV, for TiO_2, and 456.59 and 460.7 eV, for Ti_2O_3. Furthermore, the absence of metallic Ti after anodization at 25 and 50 V indicates that the surface was completely oxidized. Figure 4 shows the corresponding O1s spectra of the film. These spectra can be deconvoluted into three peaks, namely: Ti–O (~530 eV), Ti–OH (~531 eV), and H–O–H (~532 eV) [12].

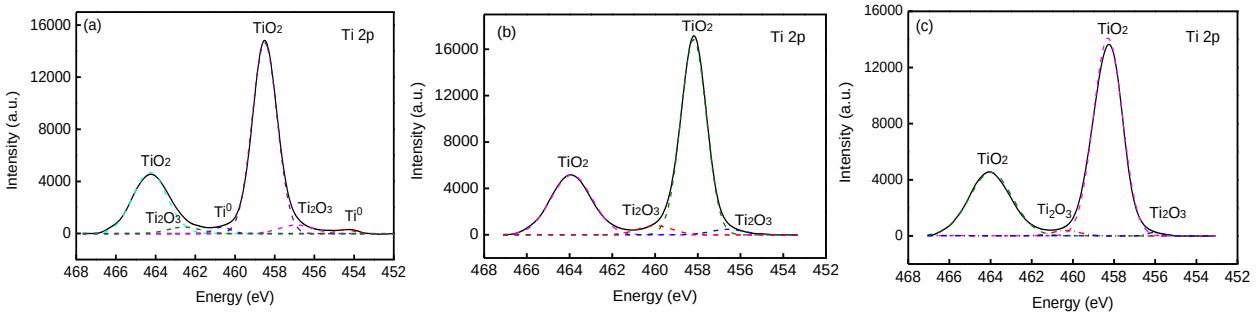

Figure 3. Ti2p XPS survey spectrum of the anodic oxide film formed under applied potentials of (a) 5 V, (b) 25 V, and (c) 50 V

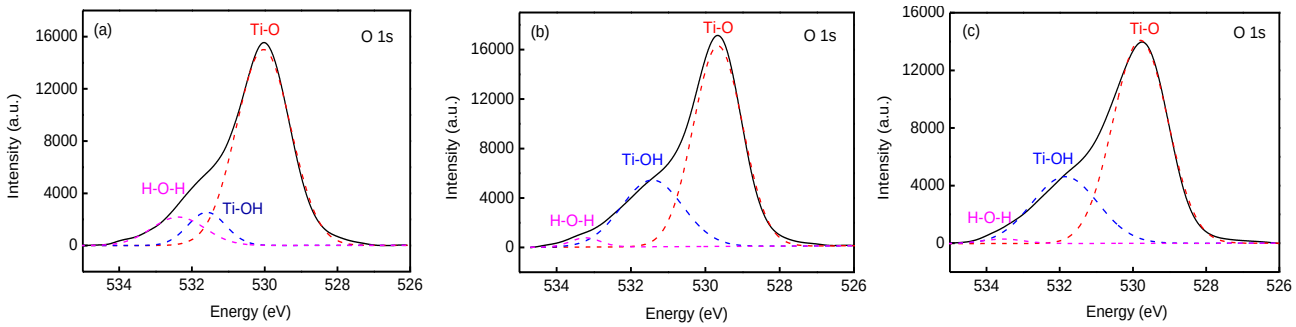

Figure 4. O1s XPS survey spectrum of the anodic oxide film formed under applied potentials of (a) 5 V, (b) 25 V, and (c) 50 V

The anodic oxides on the pure Ti surface consist mainly of TiO_2, a small amount of Ti_2O_3 and titanium hydroxide. In addition, the oxidation degree of the film increased with increasing potential, as evidenced by the intensity of the peaks shown in Fig. 3 and Fig. 4.

3.2 Electrochemical characterization

Figure 5 shows the potentiodynamic polarization curves measured after immersing the films in a NaCl solution for 30 h. The curves exhibit similar trends. The hydrogen evolution reaction of H_2O or H^+ constitutes the main process in the cathodic region. In the anodic region, the current density increases with increasing potential due to the activation polarization arising from the corrosion potential. Thereafter, the current density remains constant with increasing potential, indicating the successful formation of anodic oxide films in this region [19].

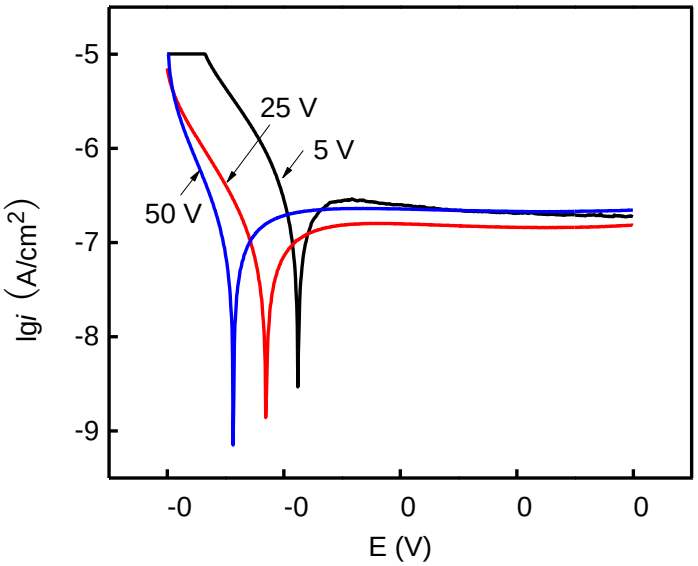

Figure 5. Potentiodynamic polarization curves of the anodic oxide films formed after 30 h of immersion in NaCl solution

The corrosion potential (E_{corr}) and corrosion current density (i_{corr}; see Table 2) can be determined via the polarization curve extrapolation method [20]. As the table shows, the anodized samples exhibit passive behavior and have low i_{corr} values. Furthermore, the E_{corr} varies only slightly, whereas i_{corr} decreases significantly with increasing potential (from 5 to 50 V). Low i_{corr} values indicate that the passive film is only slowly corroded [21], and hence, provides excellent protection to the bare metal.

Table 2. Results of the corrosion resistance test performed in 3.5 wt.% NaCl solution

Sample	Corer/mV	βa/V	βc/V	Rp/Ω.cm^2	Icorr/A.cm^{-2}
5 V	−0.176	0.15	9.57	1.6×10^{5}	3.987×10^{-7}
25 V	−0.231	2.02	10.30	6.9×10^{6}	1.058×10^{-7}
50 V	−0.287	1.85	19.3	7.4×10^{6}	9.859×10^{-8}

Figures 6 and 7 show the result of the EIS test performed after 30 h of immersion of the anodized commercially pure titanium. The Nyquist plots (Fig. 6) exhibit similar trends, i.e., an incomplete and depressed semicircle is formed in all cases [22]. In addition, the semicircles associated with Ti prepared at 5 and 25 V have almost the same diameter, but are narrower than the semicircle associated with Ti prepared at 50 V. The diameter of the semicircle is proportional to the magnitude of the polarization resistance [23–25]. Therefore, the oxide film obtained at high potential (for example, 50 V) is more resistive than those formed at lower potentials.

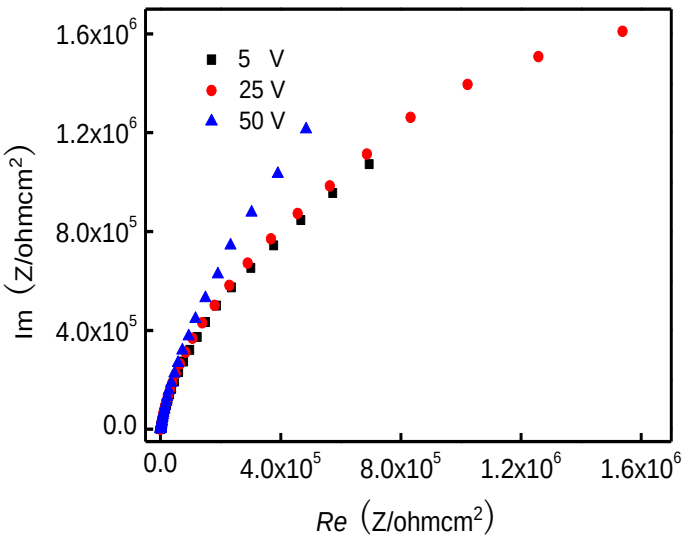

Figure 6. Nyquist plot of the anodic oxide film formed at different potentials after 30 h of immersion

Each of the Bode magnitude plots shown in Fig. 7a consist of two distinct regions. The high-frequency region (10^4–10^5 Hz) is characterized by a plateau (slope: ~0), which is correlated with the electrolyte resistance response. In the low- and mid-frequency range, the impedance varies linearly

(slope: ~1) with the frequency, consistently with the occurrence of a capacitive load [26,27]. The high-frequency region of the Bode phase diagram shown in Fig. 7b is characterized by a phase angle of ~0°, corresponding to the electrolyte resistance. Similarly, a phase angle of approximately −80° in the intermediate-frequency region is indicative of a capacitive load. A sharp peak phase angle occurs in each of the high- and low-frequency regions, consistently with the formation of a duplex passive film structure (a compact inner layer and a porous outer layer) on Ti [28].

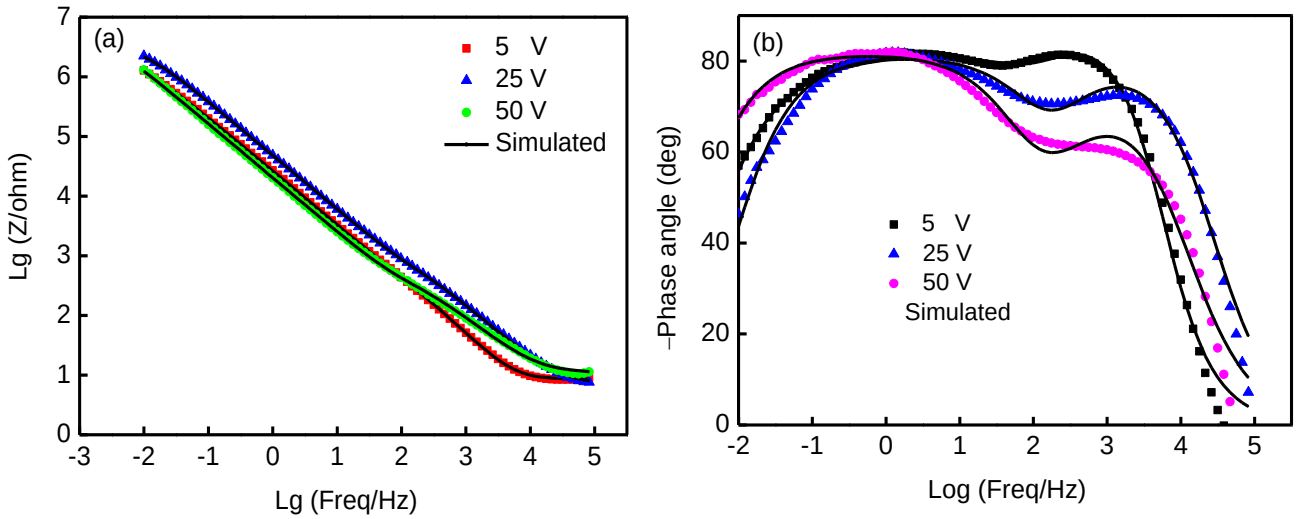

Figure 7. Bode plots of the anodic oxide film formed at different potentials after 30 h of immersion in NaCl solution: (a) Bode magnitude plots and (b) Bode phase plots

The equivalent circuit (see Fig. 8) was selected based on the EIS results and fitting of the experimental data with the ZSimpWin software. An Rs(Qp(Rp(QbRb))) circuit model with two time constants was used to fit the passive film obtained at low potential (5 V), whereas an Rs(QpRp)(QbRb) model was used for films formed at higher potentials (25 V and 50 V). In the equivalent circuit (Fig. 8), RS represents the solution resistance; *Qp* and *Qb* denote the constant phase elements [29], corresponding to the non-ideal capacitances of the porous outer layer and the compact inner layer, respectively; *Rp* and *Rb* represent the resistance of the porous outer and compact inner layer, respectively.

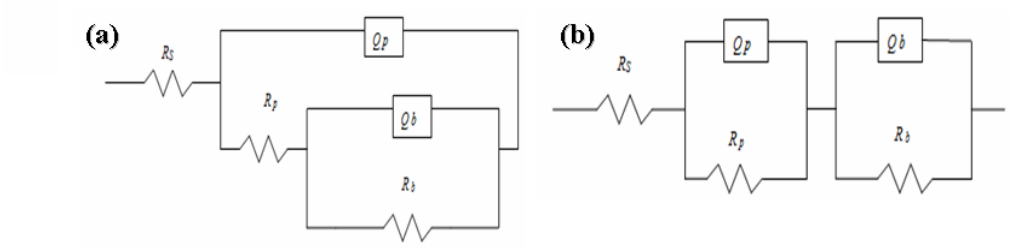

Figure 8. Equivalent circuit model

The electrochemical parameters obtained from the equivalent circuit are listed in Table 3. The low value (~10^{-3}) of χ^2 indicates that the test results correspond closely to the fitting results. Moreover, the *n* value, which is indicative of the roughness of the metal-oxide interface [30], increases with increasing smoothness of the interface. The value of R_S is only slightly affected by the processing conditions. The *Rb* values are substantially higher than their *Rp* counterparts, indicating that the corrosion resistance of the Ti passive films stems mainly from the compact inner layer. Furthermore, *Qb* decreases whereas *Rb* increases with increasing oxidation potential, indicating that the oxide film obtained at high potential is less susceptible to corrosion than those formed at low potential. Similarly, when the voltage is increased, *Qp* increases whereas *Rp* decreases, due possibly to the thinning of the porous outer layer.

Table 3. Electrical parameters obtained from the equivalent circuit of anodic films formed on TA2 pure Ti

	Electrical parameters obtained via EIS fitting							
	R_S ($\Omega\cdot cm^2$)	$Q_p\times10^{-6}$ (Fcm^{-2})	n_p	R_p ($\Omega\cdot cm^2$)	$Q_b\times10^{-6}$ (Fcm^{-2})	n_b	R_b ($\Omega\cdot cm^2$)	$\chi^2\times10^{-3}$
5 V	8.606	3.171	0.8	1288	4.267	0.8	2.99×10^6	6.27
25 V	7.217	6.088	0.8	217	3.945	0.9	3.5×10^6	2.22
50 V	8.78	9.298	0.91	203	1.26	0.83	5.02×10^6	8.03

3.3 Corrosion characterization

Table 4. Thickness of passive films calculated by the model

Samples	5 V(nm)	25 V(nm)	50 V(nm)
Thickness of porous outer layer	16.75	8.72	5.71
Thickness of compact inner layer	12.44	13.46	42.14
Total thickness	29.19	22.18	47.85

The corrosion resistance of Ti and its alloys is influenced by factors such as the composition, microstructure, structure, and environment [19]. This resistance is also significantly influenced by the thickness of the passive film. The theoretical value of the film thickness may be calculated from [31]:

$$d = \frac{\varepsilon\varepsilon_0 A}{C} \quad (1)$$

where *d*, ε, ε_0, *A*, and *C* are the thickness of the passive film, the dielectric constant of the film, the dielectric permittivity of vacuum ($\varepsilon_0 = 8.85\times10^{-12}$ F/m), the effective area of the passive region (1 cm^2), and the fitting capacitance value (which is equivalent to the capacitance Q), respectively.

Although the passive-film thickness values may be lower than the actual thickness, their values can still be used to determine the corrosion resistance of films. We assume an ε of 60 duo for the Ti passive film composed of TiO_2, Ti_2O_3, and metal Ti [27]. The calculated values are all listed in Table 4. Passive films with comparable thicknesses are obtained at 5 V and 25 V, but significantly thicker films are formed at 50 V. This indicates that the corrosion resistance improves considerably when the oxidation voltage is increased to 50 V.

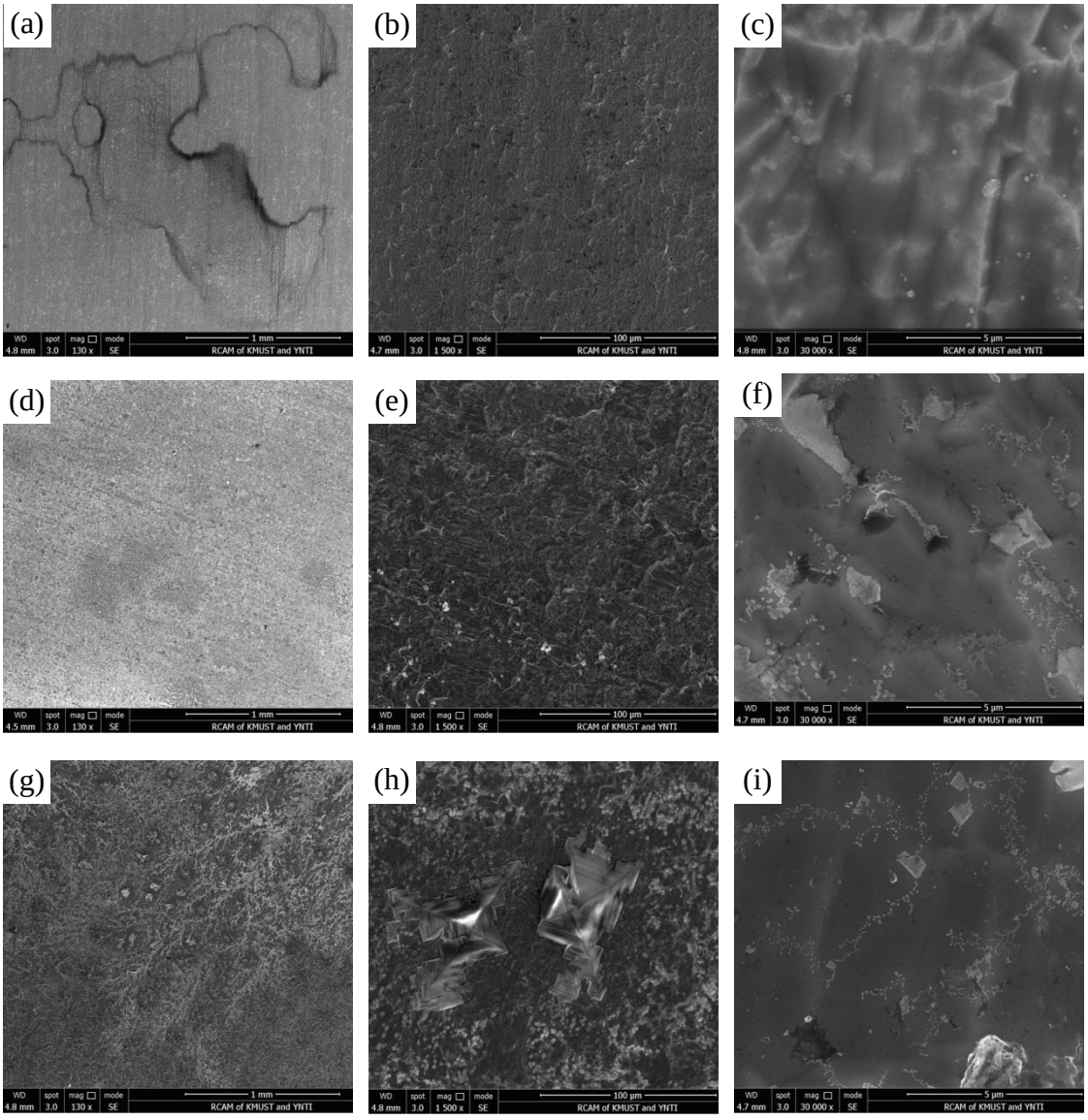

Figure 9. Surface morphologies of the anodic oxide films formed on Ti after immersion in 3.5 wt.% NaCl solution for 30 h ((a,b,c) 5 V, (d,e,f) 25 V, (g,h,i) 50 V)

Figure 9 shows surface micrographs of the anodic oxide films formed at various oxidation potentials after 30 h of immersion in a 3.5 wt.% NaCl solution at room temperature. Millimeter-long cracks occur in the surface-oxide film formed at 5 V (see Fig. 9a). A high-magnification image reveals significant corrosion patterns and micron-sized holes (Fig. 9b). Further magnifications reveal the grain structure of industrial Ti (Fig. 9c), indicating that the oxide film on the Ti surface is partially removed

during the immersion process. The surface of the film formed at 25 V is resistant to micro-cracking (Fig. 9d), but high-magnification images revealed significant corrosion patterns and a number of holes, albeit less than those formed at 5 V (Fig. 9e, f), and the surface morphology of industrial pure Ti is absent. When the oxidation potential is further increased to 50 V, a few micron-sized pores form on the surface of the film, which remains crack-free (Fig. 9g). The "pine-like" shaped regular objects shown in Fig. 9h are closely correlated with the crystallization. High-magnification images revealed that the surface of the film is very flat and has undergone only a small amount of rupturing (Fig. 9i). As in the river-like pattern of the fabric, the surface of the film formed at 50 V consists of many white, regular-shaped features.

The EDS analysis results of the oxide film immersed in NaCl solution for 30 h are shown in Fig. 10. The surface of the film formed at a potential of 5 V after immersion is composed of three main elements: Ti, O, and C (Fig. 10a), which account for mass percentages of 86.7%, 9.2%, and 4.1%, respectively. Furthermore, the oxygen content is very low, indicating that part of the film was removed by Cl^- etching, as previously suggested by the results shown in Fig. 9. C may have resulted from surface contamination. Figure 10b shows the surface EDS results of the oxide film formed when 50 V are applied after immersion. The main elements, Ti, O, Na, Cl, C, and S, account for mass percentages of 45.6%, 24.1%, 14.3%, 10.6%, 5.0%, and 0.4%, respectively. Figure 10b shows that NaCl results from the etching solution attached to the film. In fact, NaCl and TiOx were detected on the "pine-like" shaped regular crystals shown in Fig. 9h, indicating that their crystallization is induced by the high potential. The detected S stems from the anodic oxidation electrolyte, and (as previously stated) C is associated with surface contamination of the sample. Similarly, the contents of O and Ti in the film formed at high potential are higher and lower, respectively, than those of the film formed at low potential. This indicates that the oxide film is only slightly eroded and the Ti matrix remains unexposed.

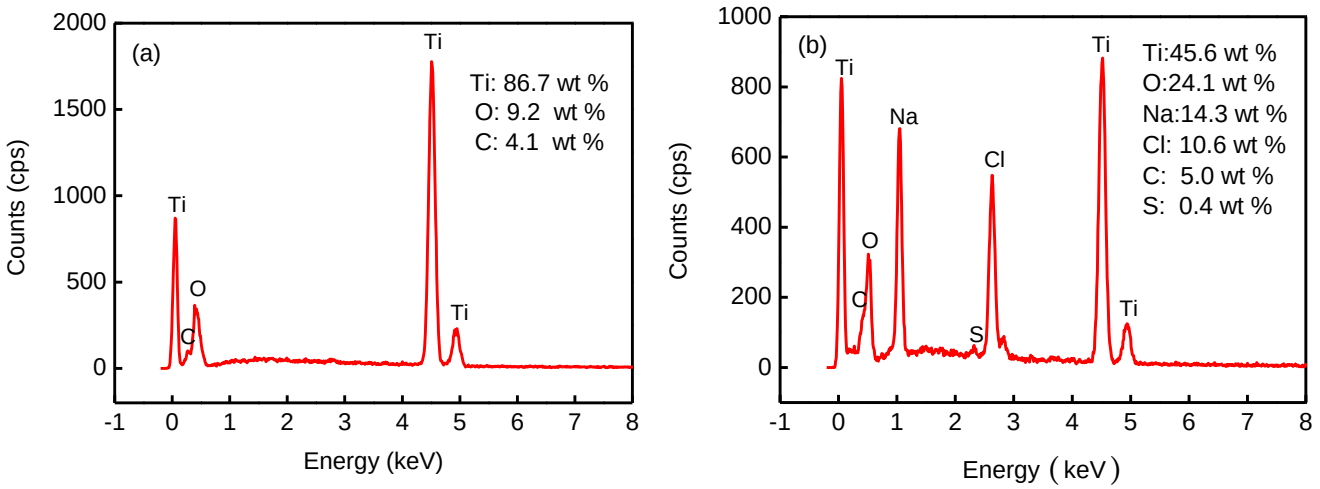

Figure 10. EDS images of the anodic oxide films formed on titanium after immersion in 3.5 wt.% NaCl solution for 30 h at (a) 5 V and (b) 50 V

The foregoing analysis reveals that defects, such as incomplete regions and thin regions, always occur in the oxide film. The defective film immersed in the NaCl solution will be initially damaged by the invasion of Cl^-, leading to the formation of corrosion holes. The TiOx in the pores dissolves under the action of Cl^-, resulting in the formation of Ti^{4+}, which is highly susceptible to hydrolysis (as shown in Reaction (2)), and consequently leading to increased acidity in the pores. This promotes the diffusion of Cl^- into the hole, resulting in an increase in the Cl^- concentration of the hole. Moreover, the corrosion products ($Ti(OH)_4$) of Ti^{4+}, resulting from the hydrolytic reaction, accumulate outside the pores, hence, the concentration of Cl^- in the cavity is substantially higher than the one outside. The low pH and high Cl^- concentration in the pores lead to increased corrosion of the defective oxide film and, in turn, to a deepening and widening of the pores. Moreover, micro-cracks will form when the nearby pores are interconnected by corrosion.

$$Ti^{4+} + 4H2O \rightarrow Ti(OH)_4 + 4H^+ \quad (2)$$

The oxide films formed at low potentials are thinner than those formed at high potentials and are therefore more susceptible to corrosion by Cl^-, resulting in the formation of millimeter-scale cracks (Fig. 9a); some of the weaker oxide films are moved due to corrosion. The film formed at high potential is thicker than those formed at low potentials and can thus hinder Cl^- penetration in the Ti matrix, thereby limiting corrosion. Therefore, the morphology of the pure Ti matrix remains unexposed, millimeter-scale cracks are limited, and only limited holes and breakages are formed (Fig. 9f and i).

4. CONCLUSIONS

The surface characteristics and electrochemical corrosion behavior of anodic oxide films formed on commercially pure Ti in 1.84 M sulfuric acid were investigated. These films exhibited hill-and-valley-like topography and consisted of nano-scale holes, which increased in number and size with increasing applied potential. The film obtained at high potential consisted mainly of TiO_2, a small amount of Ti_2O_3, and titanium hydroxide. On the other hand, the anodic oxides formed at low potential consisted of metallic Ti (in addition to TiO_2, Ti_2O_3, and titanium hydroxide), indicating that the oxidation degree of the film improved with increasing potential.

The electrochemical test results revealed that the corrosion resistance of the oxide film is mainly related to the dense inner oxide film. When the oxidation potential is increased, the resistance, *Rb*, of the inner layer increases and the capacitance, *Qb*, decreases. This indicates that the oxide film obtained at high potential is less susceptible to corrosion than those formed at low potential. The corrosion resistance of the film also depends on its thickness, which was therefore calculated for both the inner and outer films as an indicator of corrosion resistance. These calculations revealed that the films formed at 5 and 25 V have similar total thickness, but are significantly thinner than the film formed at 50 V, which exhibits better corrosion resistance than its thinner counterparts.

The possible corrosion process of the oxide film is discussed. We believe that the corrosion of the oxide film is closely related to the action of Cl^-. Some defects in the film surface immersed in NaCl solution will be damaged first, due to the invasion of Cl^-, leading to the formation of corrosion

holes. Micro-cracks are formed when adjacent pores become interconnected during corrosion. Compared with the thick film formed at high potential, the thin films formed at low potentials are more susceptible to corrosion by Cl^-, and millimeter-scale cracks are formed; in fact, some of the weaker oxide film was removed by corrosion. The aforementioned thick oxide film can hinder Cl^- penetration of the Ti matrix, thereby resulting in limited pore formation and breakage.

ACKNOWLEDGEMENTS
This work was financially supported by the Natural Science Foundation of China (No. 51665022 and 51601081).

References

1. S. A. Fadl-allah, Q. Mohsen, *Appl. Surf. Sci.*, 256(2010)5849-5855.
2. D. J. Kong, J. C. Wang, *J. Alloys Compd.*, 632(2015)286-290.
3. V. Zwilling, M. Aucouturier, E. Darque-Ceretti, *Electrochim. Acta*, 45(1999) 921-929.
4. S. Ningshen, U. K. Mudali, P. Mukherjee, A. Sarkar, P. Barat, N. Padhy, B. Raj, *Corros. Sci.*, 50(2008)2124-2134.
5. R. M. Abou Shahba, W. A. Ghannem, A. E. El-Shenawy, A. S. I. Ahmed, S. M. Tantawy, *Int. J. Electrochem. Sci.*, 6(2011) 5499-5509.
6. S. Miraghaei, M. Santamaria, F. Di Quarto, *Electrochim. Acta*, 134(2014)150-158.
7. Y. R. Smith, B. Sarma, S. K. Mohanty, M. Misra, *Electrochem. Commun.*, 19 (2012)131- 134.
8. Z. R. Zhang, Z. L. Gong, Y. Yang, *J. Phys. Chem. B.*, 108(2004) 17546-17552.
9. Q. H. Chen, H. L. Liu, Y. J. Xin, X. W. Cheng, J. Zhang, J. J. Li, P. Wang, H. J. Li, *Electrochim. Acta*, 99(2013) 152-160.
10. W. Simka, A. Sadkowski, M. Warczak, A. Iwaniak, G. Dercz, J. Michalska, A. Maciej, *Electrochim. Acta*, 56(2011)8962-8968.
11. E. Ngaboyamahina, H. Cachet, A. Pailleret, E. M. M. Sutter, *Electrochim. Acta*, 129(2014) 211-221.
12. J. H. Xing, Z. B. Xia, J. F. Hu, Y. H. Zhang, L. Zhong, *Corros. Sci.*, 75(2013)212-219.
13. S. Ningshen, M. Sakairi, K. Suzuki, T. Okuno, *Corros. Sci.*, 91(2015) 120-128.
14. Y. W. Song, D. Y. Shan, R. S. Chen, E. H. Han, *Corros. Sci.*, 51(2009)1087-1094.
15. T. Dikici, M. Toparli, *Mater. Sci. Eng. A.*, 661(2016)19-24.
16. L. Wu, J. H. Liu, M. Yu, S. M. Li, H. X. Liang, M. Q. Zhu, *Int. J. Electrochem. Sci.*, 9(2014)5012-5024 .
17. M. Sowa, K. Greń, A. I. Kukharenko, D. M. Korotin, J. Michalska, L. Szyk-Warszyńska, M. Mosialek, J. Żak, E. Pamula, E. Z. Kurmaev, S. O. Cholakh, W. Simka, *Mater. Sci. Eng. C.*, 42(2014)529- 537.
18. Y. Sano, M. Takeuchi, Y. Nakajima, H. Hirano, G. Uchiyama, Y. Nojima, S. Fujine, S. Matsumoto, *J. Nucl. Mater.*, 432(2013)475-481.
19. F. X. Xie, X. B. He, S. L. Cao, M. Mei, X. H. Qu, *Electrochim. Acta*, 105(2013)121-129.
20. M. T. Tanvir, K. Fushimi, K. Shimizu, S. Nagata, P. Skeldon, G. E. Thompson, H. Habazaki, *Electrochim. Acta*, 52(2007)6834-6840.
21. S. M. Li, X. M. Yu, J. H. Liu, M. Yu, G. L. Wu, L. Wu, K. Yang, *Int. J. Electrochem. Sci.*, 8(2013)5438-5447.
22. R. Sánchez-Tovar, R. M. Fernández-Domene, D. M. García-García, J. García-Antón, *J. Power Sources*, 286 (2015) 224-231.
23. C. Vasilescu, S. I. Drob, E. I. Neacsu, J. C. Mirza Rosca, *Corros. Sci.*, 65(2012)431-440.
24. I. Milošev, D. Blejan, S. Varvara, L. M. Muresan, *J. Appl. Electrochem.*, 43(2013) 645-658.
25. L. A. Sérgio, W. Stephan, C. Isolda, *Electrochim. Acta*, 51(2006)1815-1819.

26. M. T. Woldemedhin, D. Raabe, A. W. Hassel, *Electrochim. Acta*, 82(2012)324-332.
27. Y. Bai, S. J. Li, F. Prima, Y. L. Hao, R. Yang, *Appl. Surf. Sci.*, 258(2012) 4035-4040.
28. A. M. Fekry, R. M. EI-Sherif, *Electrochim. Acta*, 54(2009) 7280-7285.
29. F. Rosalbino, D. Macciò, G. Scavino, A. Saccone, *J. Mater. Sci. - Mater. Med.*, 23(2012)865-871.
30. D. Quintero, O. Galvis, J. A. Calderón, J. G. Castaño, F. Echeverría, *Surf. Coat. Tech.*, 258(2014)1223-1231.
31. A. A. Ghoneim, A. S. Mogoda, K. A. Awad, F. E. Heakal, *Int. J. Electrochem. Sci.*, 7(2012)6539-6554.